# Fructose–Glucose Separation in a SMB Pilot Unit: Modeling, Simulation, Design, and Operation

**Diana C. S. Azevedo and Alírio E. Rodrigues**
Laboratory of Separation and Reaction Engineering (LSRE), Faculty of Engineering, University of Porto, Rua Dr. Roberto Frias, s/n, 4200-465 Porto, Portugal

*Glucose was separated from fructose experimentally using a simulated moving-bed (SMB) adsorber. A strongly acid cationic resin of gel type ($Ca^{2+}$ form) Dowex Monosphere ($d_p = 320\ \mu m$) was used in a pilot SMB unit of twelve $26 \times 300$ mm (ID $\times$ length) columns. A recently proposed design procedure was applied to overcome the inherent strong mass-transfer resistance present in this kind of adsorbent. The fluid/solid velocity ratios in SMB sections 1, 2 and 3 leading to at least 90% product purity were followed by simulation and plotted in a 3-D parameter space. The design methodology, called "separation volume analysis," also considered the geometric parameters, as well as allowable working flow rates, temperature and pressure of the plant. Operating conditions from this procedure were used to operate the SMB unit, and the expected performance was achieved experimentally. Simulation strategies based on a true countercurrent and a real SMB were used and the predicted performance of both agreed well with experimental data. Furthermore, experimental results confirmed predictions of the separation volume analysis, which shows the potential of the technique for optimizing existing SMB equipment.*

## Introduction

The simulated moving-bed (SMB) technology was first patented by Universal Oil Products (UOP) as the Sorbex process (Broughton and Gerhold, 1961), which was applied to the petrochemical and then to the sugar industry. The SAREX process is the UOP Sorbex version of the separation of fructose–dextrose (glucose) mixtures and industrial plants have been using it since 1977 (Broughton et al., 1977). Most recently, other companies, such as Finnsugar, Illinois Water Treatment (IWT) and Mitsubishi, have commercialized SMB processes for the separation of fructose from dextrose (Gembicki et al., 1997). The key to the Sorbex technology is a rotary valve, which periodically advances the inlet and outlet streams along a sectioned column in the direction of fluid flow. An identical configuration may be achieved by using multibed units (Keller, 1995) made commercially available by such companies as Novasep (Champignelles, France) and Knauer (Berlin, Germany). With the expiration of key patents on SMB in the last few years, the SMB technology has found significantly broader applications, largely for separating fine chemicals (LeVan, 1998).

Many articles have been published about carbohydrate separation by SMB with regard to modeling, simulation, and design strategies (Ching and Ruthven, 1985a,b; 1986; Lameloise and Viard, 1993; Hassan et al., 1995; Ma and Wang, 1997; Wooley et al., 1998). Since both fructose and glucose have linear isotherms over a wide concentration range, they are an excellent test mixture to be used in developing analytical and numerical solutions for performance prediction and design purposes. Some records on experimental results for SMB separation of fructose–glucose mixtures (Hashimoto et al., 1983; Ching and Ruthven, 1985b, 1986; Ching et al., 1986; Mallmann et al., 1998) also have been published, most of them reporting using twelve columns longer than 100 cm. This way, mass-transfer resistance and dispersion effects are overcome or can be lumped into a single nonideality parameter. Hence, for linear equilibrium systems, relatively simple models (Zhong and Guiochon, 1996, 1998; Zhong et al., 1997) can be safely used for process performance prediction and design. Regarding this latter aspect, that is, the choice of suitable operating conditions for a given SMB equipment, equilibrium models, such as those reported by

Correspondence concerning this article should be addressed to A. E. Rodrigues.
D. C. S. Azevedo is on leave from GPSA, Department of Chemical Engineering, Federal University of Ceará (Brazil).

Storti et al. (1993) and Mazzotti et al. (1996, 1997), have been extremely popular. For different types of adsorption isotherms, the results reported by these authors refer to flow-rate conditions under which a SMB adsorber may achieve 100% purity for both extract and raffinate products independently on column number and dimensions. In practice, the results are only applicable for columns with a sufficiently high plate number, which can be achieved by tailoring adsorbent particle size and column dimensions in order to overcome such effects as axial mixing and mass-transfer resistances. In the case of cation exchange resins with $d_p = 320$ $\mu$m, which is the packing commonly used for sugar separation, these effects are the main sources of deviation from the results of equilibrium theory. Some authors have attempted to refine the scope of the equilibrium theory so as to include those nonideality effects into the design of operating conditions of SMB adsorbers. Pais et al (1997) shaped the regions of separation under nonideal effects by using a detailed model with intraparticle mass transfer that was described with a simple LDF approximation. It was shown that the set of values of fluid/solid flow-rate ratios in sections 2 and 3 is considerably reduced when mass-transfer effects are present, even for a constraint of 99% on product purities. Similar results were obtained by Migliorini et al. (1999). By using a complete, detailed model, they defined the regions of separation in the $m_2 \times m_3$ plane for decreasing purity requirements $(99\%, 95\%, \ldots, 60\%)$. For SMB columns having the number of theoretical stages above a threshold value (40), the regions of separation would grow larger with decreasing purity requirements as compared to the region defined by the equilibrium theory. On the other hand, for less efficient columns, the regions of separation will virtually "shrink" in comparison with the ideal region, and they may eventually not exist if the constraint on purity is too strict or the columns have a plate number far below the limiting value. Both of these works attributed values to the flow-rate ratios in sections 1 and 4 in accordance with the explicit relations defined in equilibrium theory with the given safety margin.

Therefore, using the equilibrium model as the sole design technique of the operating conditions of a given equipment might lead to overestimation of process performance, especially when the packing limits the number of theoretical stages of the columns. The correct choice of operating flow rates so as to overcome high HETP becomes a crucial aspect if geometric parameters are fixed (column number and dimensions) and mass-transfer resistance is critical. Detailed models, which take nonideality effects into account, become necessary to *filter* the findings of the equilibrium models and determine the actual conditions of separation. This statement is confirmed by the conclusions of a recently published work by Beste et al. (2000). These authors have proposed an algorithm to optimize SMB operating conditions in order to separate fructose–glucose mixtures. The equilibrium–working triangle is used as a starting point. Then, detailed true moving-bed- (TMB) and SMB-based models are further used to optimize the flow-rate/switching time in terms of purity, productivity, and solvent consumption. In the case of the present application (separation of fructose–glucose mixtures), a pertinent conclusion stated by Beste et al. (2000) is that the lowest possible internal flow rate is recommended, because it leads to small HETP and hence higher efficiency of the apparatus.

This work brings experimental results of fructose–glucose separation based on results given by a previously published design strategy (Azevedo and Rodrigues, 1999a). The methodology, called "separation volume analysis," was used to design the operating conditions of an existing SMB pilot unit that has low-efficiency columns. A constraint on product purity of both products (extract and raffinate) was set at a minimum of 90%. Results of this methodology are presented in a 3-dimensional (3-D) framework based on the fluid–solid velocity ratios in sections 1, 2 and 3. Operating points, which fulfill the purity restrictions, were chosen as conditions to operate the SMB. Experimental steady-state concentration profiles and average product (extract and raffinate) concentrations were compared with those obtained from a TMB model. The transient evolution of profiles and the periodic character of the steady state of a simulated moving bed were examined by using a real SMB model and comparing its solution with experimental data. In all cases, good agreement between theory and experiment was obtained and the separation volume analysis could be validated with key experiments.

## Mathematical Models for SMB Unit Performance Prediction

The performance of a SMB unit can be assessed essentially by using either one of two modeling strategies: (1) by considering it as an equivalent TMB unit in which both the solid and liquid phases move in opposite directions; and (2) by treating it as a real SMB unit in which the solid phase is fixed with periodic port switching. Figure 1 shows both a TMB and a SMB.

The TMB modeling strategy requires much less computational effort to be solved, and steady state can be calculated directly. It is a much more suitable approach for design methodologies that involve successive simulations. In this

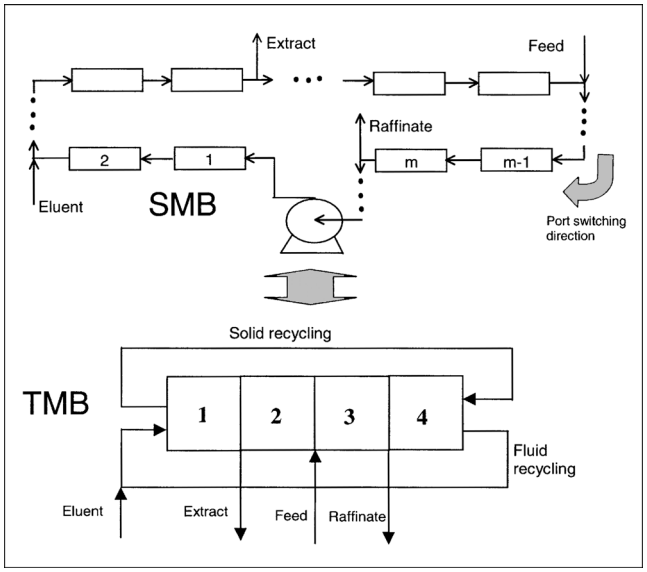


**Figure 1. Representation of a SMB and the equivalent TMB.**

work, the TMB model was used for steady-state calculations only in order to shape the borders of the regions of separation as a function of the velocity ratios in sections 1, 2, and 3. A double linear driving force (Azevedo and Rodrigues, 1999b) was assumed to describe mass transfer in the pores (rate constant $= k_p$) and in the microparticles (rate constant $= k_\mu$) of the adsorbent particle.

The SMB modeling strategy is more precise than the previous one, since it depicts the actual physical equipment operation. It allows the visualization of the axial movement of concentration profiles and the variations in extract and raffinate concentration within a period. However, it demands considerably higher computational effort than the TMB strategy, especially when a large number of columns are involved. Steady-state performance may only be assessed by calculation of the transient response. The differential mass-balances equations formulated for both models are summarized in Table 1. The equations in the left column apply to a chemical species $i$ in a TMB section $j$. The mathematical model under the SMB strategy is shown in the left column where the equations apply to a chemical species $i$ in a SMB column $k$. For this latter model, intraparticle mass transfer is represented by a single LDF approximation, so that the required computational time is not too high and mass-balance errors can be minimized.

## Choice of SMB Operating Conditions

Designing the operating conditions of an existing SMB plant consists of choosing adequate flow rates for each zone and rotation period, which yield acceptable and robust separation at minimum cost. In other words, it is desirable to maximize the purity and recovery of products making effective use of the adsorbent while minimizing the solvent consumption. Therefore, the design procedure may intend to minimize and/or maximize one or more performance criteria. As far as this work is concerned, the design methodology used attempted to find a compromise between section flow-rate ratios that would result in purities of not less than 90% for both extract and raffinate. Productivity and concentration of target chemical species in each product are also performance parameters that are examined in this work. They are defined as:

**Table 1. Models Used in This Work to Predict SMB Performance**

| TMB-Based Model | SMB-Based Model |
|---|---|
| • Differential mass balances (steady state) in bulk fluid phase, pore fluid phase, and solid phase for species $i$ in section $j$: $\frac{\gamma_j}{Pe_j}\frac{\partial^2 C_{i,j}}{\partial x^2} - \gamma_j\frac{\partial C_{i,j}}{\partial x} - \frac{(1-\epsilon)}{\epsilon}\left[\frac{Bi_{mj}}{5+Bi_{mj}}\alpha_{pj}(C_{i,j}-\overline{C}_{i,j})\right]=0$ $\frac{\partial \overline{C}_{p_{i,j}}}{\partial x} + \frac{Bi_{mj}}{5+Bi_{mj}}\frac{\alpha_{pj}}{\epsilon_p}(C_{i,j}-\overline{C}_{p_{i,j}}) - \frac{\alpha_{\mu j}}{\epsilon_p}[K_i\overline{C}_{p_{i,j}} - \langle\overline{q}\rangle_{i,j}]=0$ $\frac{\partial\langle\overline{q}\rangle_{i,j}}{\partial x} + \alpha_{\mu_j}[K_i\overline{C}_{p_{i,j}} - \langle\overline{q}\rangle_{i,j}]=0,$ where $x = z/L_j$. | • Differential mass-balances, global, and in solid phase for species $i$ in column $k$: $\frac{\partial C_{i,k}}{\partial\theta} + \nu\frac{\partial\overline{q}_{i,k}}{\partial\theta} = \frac{\Psi_k}{Pe_k}\frac{\partial^2 C_{i,k}}{\partial'\chi^2} - \Psi_k\frac{\partial C_{i,k}}{\partial\chi}$ $\frac{\partial\overline{q}_{i,k}}{\partial\theta} = \alpha_i\frac{Bi_{m_k}}{5+Bi_{m_k}}(\overline{q}^*_{i,k}-\overline{q}_{i,k})$ $\overline{q}^*_{i,k} = K'_iC_{i,k},$ where $\chi = z/L_c$ and $\theta = t/t^*$ |
| • Boundary conditions: $C^{in}_{i,k} = C_{i,j}(0) - \frac{1}{Pe_j}\frac{\partial C_{i,j}}{\partial x}\quad \frac{\partial C_{i,j}}{\partial x}(1)=0$ $\overline{C}_{p_{i,j}}(1) = \overline{C}_{p_{i,j+1}}(0)\qquad \langle\overline{q}\rangle_{i,j}(1) = \langle\overline{q}\rangle_{i,j+1}(0)$ | • Boundary conditions: $C^{in}_{i,\lambda} = C_{i,k}(0,\theta) - \frac{1}{Pe_k}\frac{\partial C_{i,k}}{\partial\chi}$ $\frac{\partial C_{i,k}}{\partial\chi}(1,\theta)=0$ |
| • Dimensionless parameters: $\gamma_j = \frac{U'_{Fj}}{U_S}\qquad Pe_j = U'_{F_j}L/D_{ax_j}$ $\alpha_{pj} = \frac{k_pL_j}{U_S}\qquad \alpha_{\mu j} = \frac{k_\mu L_j}{U_S}$ $Bi_{mj} = \frac{k_{fj}R_p}{D_{pe}}$ | • Initial conditions: $C_{i,k}(\chi,0) = C^0_{i,k}(\chi)\quad \overline{q}_{i,k}(\chi,0) = \overline{q}^0_{i,k}(\chi)$ |
| | • Dimensionless parameters: $\Psi_k = U_{F_i}t^*/L_c\qquad \alpha_i = k_{h_i}t^*$ where $k_h = \left(\frac{K+\epsilon_p}{k_p} + \frac{K}{k_\mu(K+\epsilon_p)}\right)^{-1}$ and $K' = K + \epsilon_p$. |
| • Node balances: $C^{in}_{i,1} = \frac{Q'_4}{Q'_4+Q_E}C_{i,4}(1)\qquad C'^{in}_{i,2} = C_{i,1}(1)$ $C^{in}_{i,3} = \frac{Q'_2}{Q'_3}C_{i,2}(1) + \frac{Q_F}{Q'_3}C_{i,F}\quad C'^{in}_{i,4} = C_{i,3}(1)$ | • Node balances: $C^{in}_{i,k} = C_{i,k-1}(1,\theta)$, *except if column follows feed or eluent port. In that case,* $C^{in}_{i,k} = [Q_FC_{i,F} + Q_2C_{i,k-1}(1,\theta)]/Q_3$ $C^{in}_{i,k} = Q_4C_{i,k-1}(1,\theta)/Q_1$, *respectively* |

PRX = extract productivity

$$= \frac{\text{kg of fructose obtained in the extract}}{\text{m}^3 \text{ adsorbent} \times \text{hour}}$$

PRR = raffinate productivity

$$= \frac{\text{kg of glucose obtained in the raffinate}}{\text{m}^3 \text{ adsorbent} \times \text{hour}}$$

$CX_{FR}$ = Fructose concentration in the extract $\left(\text{kg/m}^3\right)$

$CR_{GL}$ = Glucose concentration in the raffinate $\left(\text{kg/m}^3\right)$.

Consider a SMB adsorber used to separate a mixture of fructose (FR) and glucose (GL). The equilibrium theory states that, for both extract and raffinate of 100% purity to be collected, the following constraints on the section velocity ratios must be met (Ruthven, 1984)

$$\gamma_1 > \nu K'_{FR} \tag{1}$$

$$\nu K'_{GL} < \gamma_2 < \nu K'_{FR} \tag{2}$$

$$\nu K'_{GL} < \gamma_3 < \nu K'_{FR} \tag{3}$$

$$\gamma_4 < \nu K'_{GL}, \tag{4}$$

where $\nu = (1-\epsilon)/\epsilon$ and $\gamma_3 > \gamma_2$.

These constraints define separation in a TMB and equivalent SMB, for a linear equilibrium binary system in the absence of dispersion and mass-transfer effects. This region corresponds to the triangle *CWD* shown in Figure 2, inside which any ($\gamma_2$, $\gamma_3$) pair yields separation, provided the constraints on $\gamma_1$ and $\gamma_4$ are not violated. When mass-transfer resistances are significant, however, the constraints are not as explicit as in Eqs. 1 to 4. The separation region is expected to become narrower, and the new constraints should be dependent on mass-transfer rate constants. To find this new separation region, it is first necessary to define the minimum purity required and then to perform successive simulations within the equilibrium triangle in order to map the regions in which the desired performance is obtained. In previous work (Azevedo and Rodrigues, 1999a), we have shown that this region is also dependent on the section 1 velocity ratio and how close to the equilibrium minimum bound the equipment is operated. In this work, we have used the following procedure to define the operating conditions to be used in the experiments:

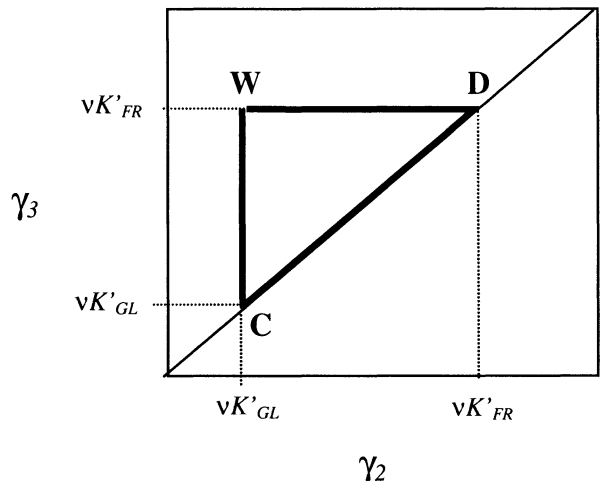


**Figure 2. Region of complete separation for a fructose–glucose mixture, according to the equilibrium model.**

1. Due to the high mass-transfer limitations imposed by the resin, it was desirable to have as low flow rates (as high column residence times) as the equipment recycling pump could possibly deliver with accuracy. For the LICOSEP 12-26 (by Novasep) pilot unit, this value was $4\times10^{-7}$ $\text{m}^3/\text{s}$ and it was taken as the flow rate in section 4.

2. By assigning a value to $\gamma_4$ of 70% of the maximum bound as given in Eq. 4, the rotation period $t^*$ could be calculated from the following equation

$$\gamma_4 = 0.7\nu K'_{GL} = \frac{Q_4 t^*}{\epsilon V_c} - 1. \tag{5}$$

3. For increasing values of $\gamma_1$, starting from the minimum equilibrium bound (Eq. 1), the region of separation (both product purities above 90%) was determined by simulation in $\gamma_2 \times \gamma_3$ planes. A robust operation point ($\gamma_1$, $\gamma_2$, $\gamma_3$) was chosen so that operational fluctuations in the section flow rates would not disturb the unit performance significantly.

## Results and Discussion

### *Experimental set up*

All experimental work was performed in a SMB pilot unit LICOSEP 12-26, manufactured by Novasep (Vandoeuvre-dès-Nancy, France). Twelve columns of Superformance SP $300\times26$ (length$\times$ID, mm), made by Götec Labortechnik (Mühltal, Germany), packed with the cationic resin Dowex Monosphere 99/Ca (Sigma) were connected to the SMB pilot unit. Each column was jacketed to ensure temperature control and the jackets were connected to one another by silicone hoses and to a thermostat bath (Lauda). Operating temperatures ranged from 20°C to 60°C. Located between every two columns was a four-port valve that was actuated by the control system. When required, the valves allowed either pumping of feed/eluent into the system or withdrawal of extract/raffinate streams. Each of the inlet (feed and eluent) and outlet (extract and raffinate) streams was pumped by means of Merck-Hitachi HPLC pumps. The recycling pump was a positive-displacement diaphragm pump, which could deliver flow rates as low as 20 mL/min and as high as 120 mL/min. The maximum allowable pressure was 60 bar. Between the twelfth and first column was a six-port valve, which was used to collect samples for internal concentration profile measurements.

### *Model parameter measurements*

The dimensionless numbers present in the model equations presented previously were calculated from kinetic, equilibrium, and dispersion parameters measured experimentally, as described in previous work (Azevedo and Rodrigues, 2000).

**Table 2. Model Parameters Measured Experimentally**

| | $T = 30$°C | | $T = 50$°C | |
|---|---|---|---|---|
| Parameter | Glucose | Fructose | Glucose | Fructose |
| $Pe$* | 500 | | | |
| $Bi_m$** | 200 | | 300 | |
| $\epsilon$ | 0.4 | | | |
| $\epsilon_p$ | 0.1 | | | |
| $K$ | 0.18 | 0.5 | 0.17 | 0.43 |
| $K' = K + \epsilon_p$ | 0.28 | 0.6 | 0.27 | 0.53 |
| $\frac{(1-\epsilon)}{\epsilon} K'$ | 0.42 | 0.9 | 0.405 | 0.795 |
| $k_p, s^{-1} (\times 10^2)$ | 3.33 | 3.33 | 4.17 | 4.17 |
| $k_\mu, s^{-1} (\times 10^2)$ | 1.33 | 1.33 | 2.17 | 2.17 |
| $k_h, s^{-1} (\times 10^2)$ | 1.767 | 1.25 | 3.15 | 2.217 |

*Average Peclet number measured for one individual SMB column (0.29 m) in the range of $4-6.5 \times 10^{-7}$ m$^3$/s.
**External-film mass-transfer coefficient estimated from Thoenes and Kramers' correlation (1958).

Table 2 summarizes the obtained parameters for the temperatures of 30 and 50°C.

### *Choice of SMB operating conditions*

The volumes of separation at 30° and 50°C for the LICOSEP SMB pilot unit were shaped by simulation according to the procedure described previously. For both plots, the simulations were performed assuming $4 \times 10^{-7}$ m$^3$/s (24 mL/min) as the flow rate in section 4. The switching times used were calculated from Eq. 5, and were equal to 199.2 and 197.7 s at 30 and 50°C, respectively. Since in practice $K'_{GL}$ does not change at 30 and 50°C, the switching time was taken to be 198 min for the calculations at both temperatures. The separation volumes obtained at 30 and 50°C are shown in Figures 3a and 3b, respectively. They are shown as polygons obtained for various distinct values of $\gamma_1$, starting from the minimum equilibrium bound. It can be verified that the separation volume obtained for 50°C is much larger than that obtained at 30°C. For the sake of clarity, these separation volumes are also represented in 2-D $\gamma_2 \times \gamma_3$ plots for different values of $\gamma_1$ in Figures 4a and 4b. The highest value of $\gamma_1$ in each plot is that above which the area of separation has an unchanging shape. In practice, increasing $\gamma_1$ means using larger eluent flow rates, which enables more combinations of operating conditions in order to achieve the desired purities. However, higher eluent flow rates also lead to more diluted products, which is undesirable if, for instance, one intends to obtain fructose syrups. From a certain point on, further increases in eluent flow rate do not contribute to the expansion of the area of separation, and that is an appropriate condition to carry out an experiment. By comparing the plots obtained at 30 and 50°C, it is clear that better performances can be achieved at 50°C at the expense of less eluent. Moreover, by using temperatures up to 70°C, microbial growth is inhibited and fluid viscosity is decreased. These can be appropriate factors when working in a high sugar concentration range. Hence, we have chosen to operate the SMB unit at 50°C. As for the choice of the ($\gamma_2$, $\gamma_3$) operating point, it is desirable to have as high throughputs as possible. This means choosing an operating point close to vertex O, shown in Figure 4. The operating point (0.5, 0.68) was selected to carry out the following SMB experiments.

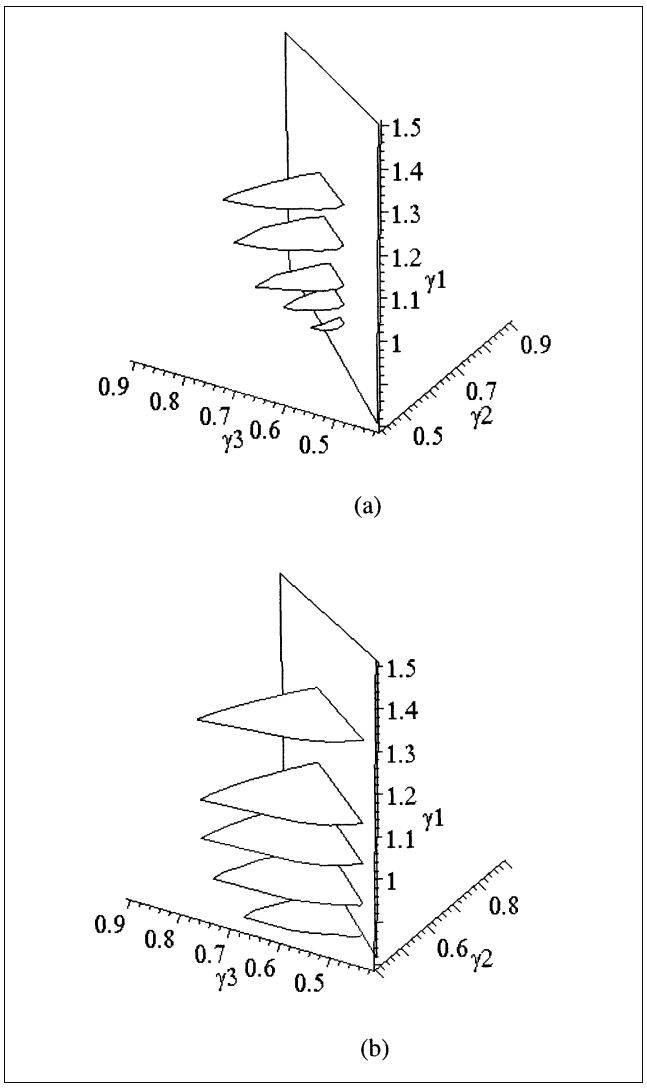


**Figure 3. Separation volumes (both product purities above 90%) at (a) 30°C and (b) 50°C, for fructose–glucose separation on LICOSEP 12–26 SMB pilot unit using Dowex Monosphere cationic resin.**

Process parameters used in the simulations are those described in Table 2.

### *SMB experiments*

Four experiments for the separation of fructose–glucose mixtures in a SMB were carried out. The operating conditions of these experiments, identified as runs A, B, C, and D, are summarized in Tables 3 to 6, respectively. Each table also compares performance parameters obtained experimentally with those predicted by simulation. In all cases, the predicted parameters were obtained by numerical simulation using the TMB model, except for Table 6, which also shows predicted results from the real SMB model.

In all experiments the feed concentration was 40 kg/m$^3$ for each sugar. Switching time, feed, and raffinate flow rates were the same and equal to 198 s, $0.56 \times 10^{-7}$, and $1.21 \times 10^{-7}$ m$^3$/s, respectively. There were three columns per section. By

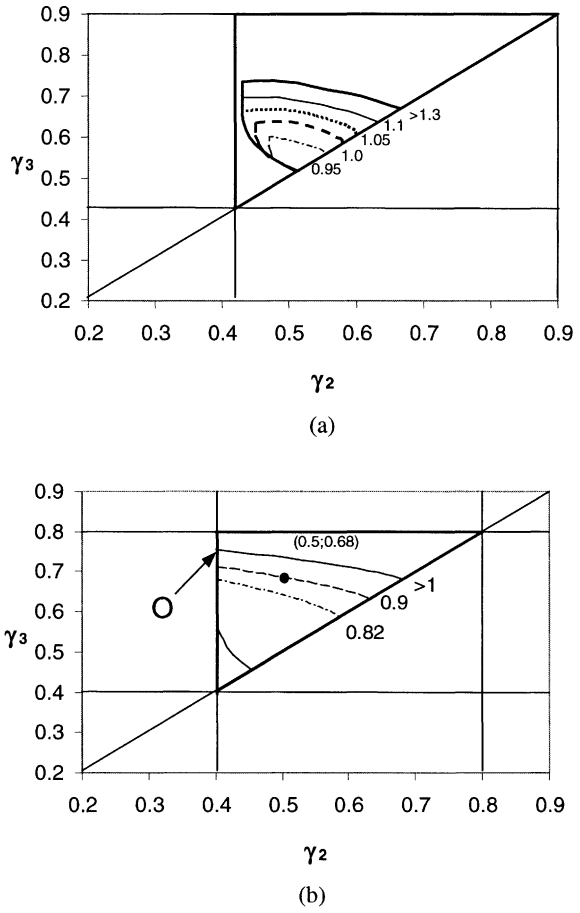


**Figure 4. Separation volumes represented in terms of projected areas on a $\gamma_2 \times \gamma_3$ plane for different $\gamma_1$ values at (a) 30°C and (b) 50°C.**

varying $\gamma_1$, different eluent and extract flow rates were tested. The system reached its periodic steady state in the 10th cycle. From that point on, the average product concentration collected for a whole cycle remained unchanged, and global mass balances of both sugars were verified (amount that enters = amount that leaves).

In run A, the velocity ratio in section 1 is 0.82, which is very close to the minimum equilibrium bound of 0.795, as shown in Table 3. In fact, by examining Figure 4b, one can verify that at $\gamma_1 = 0.82$, the point (0.5, 0.68) lies in the region of pure extract only (purity above 90%). The obtained experimental purities confirm this. As shown in Table 2, there is good agreement between theoretical and experimental performance. Figure 5 shows the concentration profile measured at the 15th cycle. Each point (white) was sampled at 50% of each of the 12 periods of a cycle. The simulated profile obtained from the steady-state TMB model, represented by unbroken lines, predicts well the experimental data. The black circle and triangle represent the average concentration of extract and raffinate collected for the whole 15th cycle.

The following experiment, run B, was carried out using a larger eluent flow rate. The velocity ratio $\gamma_1$ was increased to 0.9, as can be seen in Table 4. The table also shows the other operating conditions and the performance parameters obtained. The raffinate purity is greater in comparison with run A; however, it is still below 90%. In this situation, the pair (0.5, 0.68) in a $\gamma_2 \times \gamma_3$ plane lies right on the border of the separation region, as can be checked in Figure 4b. Should any fluctuations in section flow rate happen, then the desired performance is not likely to be achieved. Besides, the area of separation was defined using a TMB steady-state model, which usually results in more optimistic predictions of the

**Table 3. Operating Conditions and Process Parameters for Run A**

| SMB Oper. Flow Rate $\times 10^7$ m$^3$/s | Performance Parameter | Exp. | Pred. |
|---|---|---|---|
| $Q_1 = 5.67$ $\gamma_1 = 0.82$ | PUX, % | 95.7 | 97.9 |
| $Q_2 = 4.65$ $\gamma_2 = 0.50$ | PUR, % | 85.5 | 86.1 |
| $Q_3 = 5.21$ $\gamma_3 = 0.68$ | PRX, kg/m$^3$·h | 5.74 | 5.76 |
| $Q_4 = 4$ $\gamma_4 = 0.29$ | PRR, kg/m$^3$·h | 6.68 | 6.82 |
| $Q_E = 1.67$ | $CX_{FR}$, kg/m$^3$ | 17.43 | 17.41 |
| $Q_X = 1.02$ | $CR_{GL}$, kg/m$^3$ | 16.99 | 17.28 |

**Table 4. Operating Conditions and Process Parameters for Run B**

| SMB Oper. Flow Rate $\times 10^7$ m$^3$/s | Performance Parameter | Exp. | Pred. |
|---|---|---|---|
| $Q_1 = 5.91$ $\gamma_1 = 0.90$ | PUX, % | 96.9 | 97.9 |
| $Q_2 = 4.65$ $\gamma_2 = 0.50$ | PUR, % | 87.8 | 90.2 |
| $Q_3 = 5.21$ $\gamma_3 = 0.68$ | PRX, kg/m$^3$·h | 6.14 | 6.27 |
| $Q_4 = 4$ $\gamma_4 = 0.29$ | PRR, kg/m$^3$·h | 7.00 | 7.06 |
| $Q_E = 1.91$ | $CX_{FR}$, kg/m$^3$ | 14.88 | 15.27 |
| $Q_X = 1.26$ | $CR_{GL}$, kg/m$^3$ | 17.78 | 17.28 |

**Table 5. Operating Conditions and Process Parameters for Run C**

| SMB Oper. Flow Rate $\times 10^7$ m$^3$/s | Performance Parameter | Exp. | Pred. |
|---|---|---|---|
| $Q_1 = 6.21$ $\gamma_1 = 1.00$ | PUX, % | 94.9 | 98 |
| $Q_2 = 4.65$ $\gamma_2 = 0.50$ | PUR, % | 92.7 | 92.1 |
| $Q_3 = 5.21$ $\gamma_3 = 0.68$ | PRX, kg/m$^3$·h | 6.66 | 6.58 |
| $Q_4 = 4$ $\gamma_4 = 0.29$ | PRR, kg/m$^3$·h | 6.54 | 6.68 |
| $Q_E = 2.21$ | $CX_{FR}$, kg/m$^3$ | 13 | 12.99 |
| $Q_X = 1.56$ | $CR_{GL}$, kg/m$^3$ | 16.19 | 16.93 |

**Table 6. Operating Conditions and Process Parameters for Run D**

| SMB Oper. Flow Rate $\times 10^7$ m$^3$/s | Performance Parameter | Exp. | Pred. |
|---|---|---|---|
| $Q_1 = 6.38$ $\gamma_1 = 1.05$ | PUX, % | 96.5 | 97.9 (96.2)* |
| $Q_2 = 4.65$ $\gamma_2 = 0.50$ | PUR, % | 91.2 | 93.2 (91.5) |
| $Q_3 = 5.21$ $\gamma_3 = 0.68$ | PRX, kg/m$^3$·h | 6.47 | 6.74 (6.80) |
| $Q_4 = 4$ $\gamma_4 = 0.29$ | PRR, kg/m$^3$·h | 7.10 | 7.12 (7.23) |
| $Q_E = 2.38$ | $CX_{FR}$, kg/m$^3$ | 11.44 | 11.99 (11.76) |
| $Q_X = 1.73$ | $CR_{GL}$, kg/m$^3$ | 18.71 | 18.05 (17.82) |

*Values in parentheses were obtained from simulations using the SMB model.

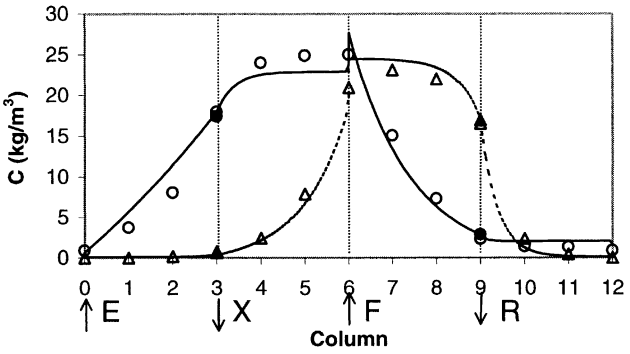


**Figure 5. Internal concentration profile: experiment at the 15th cycle vs. simulation using a TMB steady-state model.**

The curves are simulated data. Δ, ○ are glucose and fructose concentrations, respectively, sampled at 50% of each period of the 15th cycle; ▲, ● are glucose and fructose concentrations, respectively, measured from the extract and raffinate products collected for a full cycle. Operating conditions are those described in Table 3.

extract purity than are made by the SMB transient model (Pais et al., 1998).

Figure 6a illustrates the experimental concentration profile of fructose and glucose sampled at 50% of each period of the 15th cycle. The continuous lines are simulated using the steady-state TMB model. Like the plot shown in Figure 5, there is very good agreement between theory and experiment. However, from Tables 2 and 3, a difference between experimental and predicted product purities can be observed. This is due to the underestimation of the contaminant species in both extract and raffinate. Figures 6b and 6c show this effect. The points represent the measured concentration of the products collected for a whole cycle at the first, third, fifth and seventh cycle. The circles stand for fructose and the triangles stand for glucose. The thin and thick lines were obtained from the simulation using the transient SMB model, and they represent local and average concentrations, respectively, measured over a cycle. For both extract and raffinate, the amount of contamination is actually greater than that predicted. The cause of this discrepancy can be a common piece of tubing, which is part of the four-port valve located between every two columns. Every time the extract leaves a column, it mixes with a 0.1-mL volume of raffinate, and vice versa. Therefore, this discrepancy tends to be negligible the longer the cycle is and the larger product flow rates are.

In runs C and D, $\gamma_1$ is further increased to 1 and 1.05. The plot on Figure 4b shows that the separation areas predicted for these cases should be the same. As expected, both product purities are above 90%. This is shown in Tables 5 and 6, which summarize the main performance parameters obtained in the two runs. In general, all performance parameters in these two runs are very similar. Since fructose has a higher added value than glucose, the latter usually being recycled for isomerization, there are no advantages in further increases in $\gamma_1$. Using larger eluent flow rates would slightly raise extract purity, but cause undesired dilution as well.

Figure 7 shows the experimental concentration profile obtained for run C, as compared with the theoretical curves as calculated from a TMB model. Unlike the previous profiles

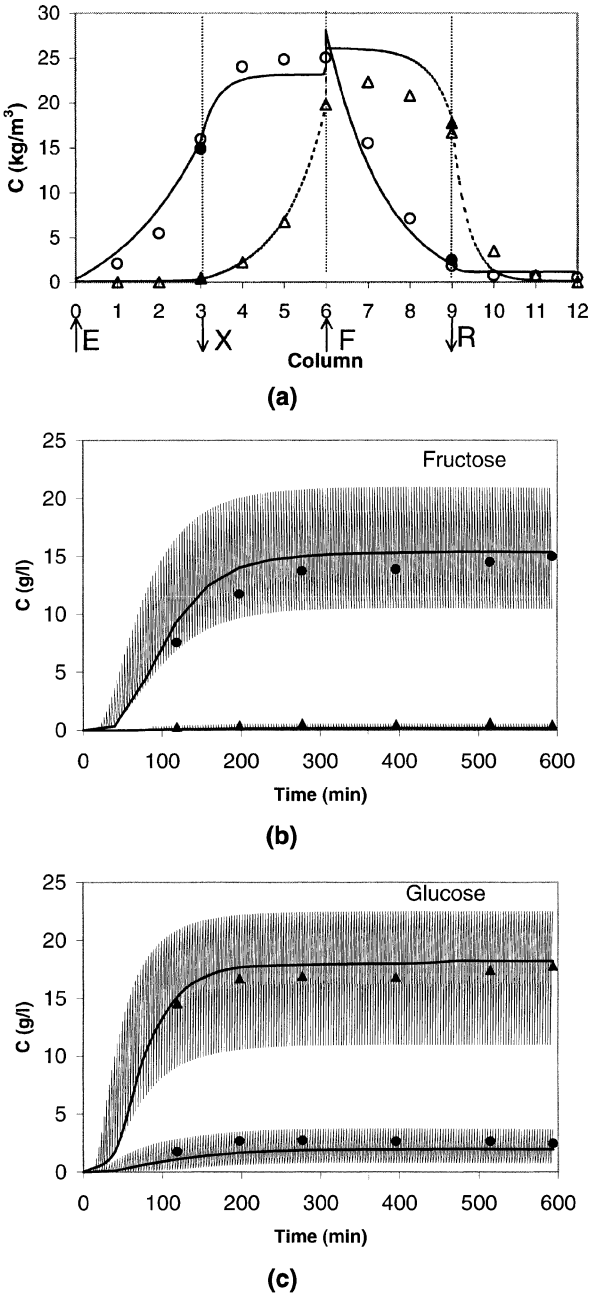


**Figure 6. Internal concentration profile: (a) experiment at the 15th cycle vs. simulation using a TMB steady-state model; (b) simulated (transient SMB model) evolution of local extract concentrations and experimental vs. simulated cycle average concentrations; (c) same as (b) for raffinate concentrations.**

The curves are simulated data. Δ, ○ are glucose and fructose concentrations, respectively, sampled at 50% of each period of the 15th cycle; ▲, ● are glucose and fructose concentrations, respectively, measured from the extract and raffinate products collected for a full cycle. Operating conditions are those described in Table 4.

shown in Figures 5 and 6, concentration of both species in sections 1 and 4 is nearly zero. In other words, eluent and

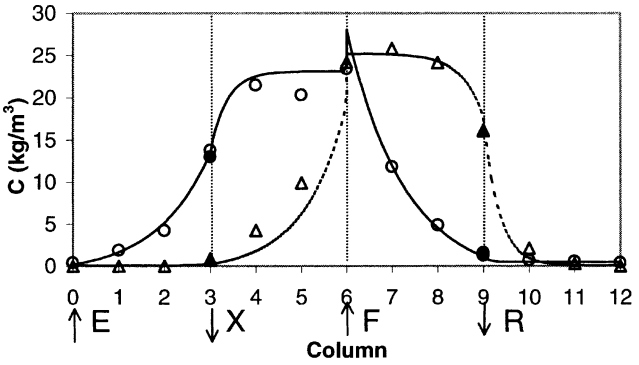


**Figure 7. Internal concentration profile: experiment at the 15th cycle vs. simulation using a TMB steady-state model.**

The curves are simulated data. Δ,○ are glucose and fructose concentrations, respectively, sampled at 50% of each period of the 15th cycle; ▲,● are glucose and fructose concentrations, respectively, measured from the extract and raffinate products collected for a full cycle. Operating conditions are those described in Table 5.

adsorbent are both regenerated and cross-contamination is decreased. Again, experimental process performance is somewhat poorer than predicted from a TMB model. Figure 8 shows experimental profiles sampled at 25%, 50%, 75%, and 100% of each period of the 15th cycle under the operating conditions described for run D. The axial movement of the concentration fronts can be verified. The curves were obtained from simulation using a transient SMB model after periodic steady state had been reached. Experimental data agree closely with that predicted by simulation. The compatibility between theory and experiment can also be verified in Table 6. Predicted parameters include those obtained both by the TMB and the SMB models. Product purities obtained from the SMB model are slightly lower than the ones predicted by the TMB model, and they were closer to the experimental values. However, for simulations using the SMB model, the cyclic steady state took 15 cycles to be reached, which requires 600 min of processing time on a Pentium II 300-MHz processor. The TMB model was solved in one minute using the same processor. Therefore, the TMB model provides a fast and relatively accurate prediction of the steady-state performance of a given SMB plant, which is enough to define its separation volume.

## Conclusions

The present work shows experimental data for the SMB separation of a glucose–fructose mixture, which validates the design methodology of "separation volumes," described in previous work (Azevedo and Rodrigues, 1999a). This methodology can be used to design the operating conditions of existing SMB pilot units that have low-efficiency columns. In such cases, design strategies based only on equilibrium models are not likely to give accurate results, and plants can eventually be oversized. For a given SMB unit, the plant operating limitations were taken into consideration and a constraint on the purity of both products (extract and raffinate) was set at a minimum of 90%. Results of this methodology are presented in terms of $\gamma_2 \times \gamma_3$ plots for various values of

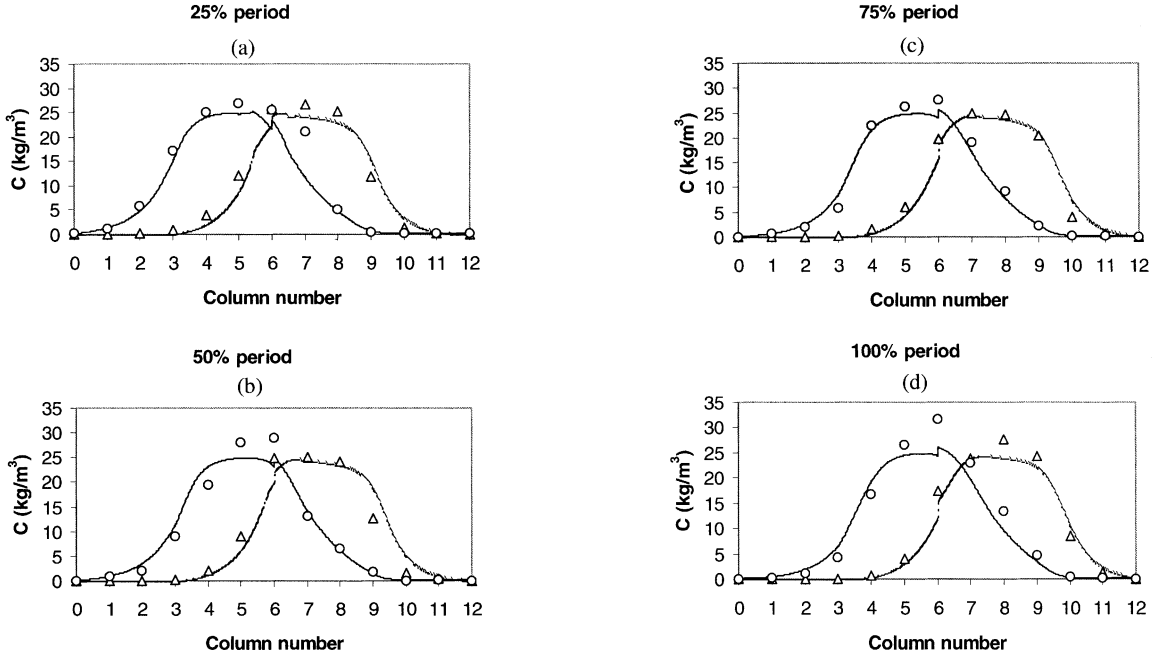


**Figure 8. SMB profiles at different moments within a period.**

Operating conditions are those described in Table 6. Experimental profiles were sampled at cyclic steady state at (a) 25% of a switching time; (b) 50%; (c) 75%; (d) 100%. Curves are simulated steady-state concentration profiles as calculated from a real SMB model. Δ,○ are glucose and fructose concentrations, respectively.

$\gamma_1$. Operating points that fulfill the purity restrictions were chosen as conditions for operating the SMB. The experimental results obtained at the conditions chosen from this methodology agree well with theoretical predictions. Detailed mathematical models based on a TMB and a real SMB were used, and simulated results were in agreement with experimental data. As a conclusion, the separation volumes methodology proved to be a useful SMB design tool in achieving desired product purity and dilution requirements.

## Acknowledgments

The authors thank CAPES (proc. 1140/96-5), the Ministry of Education of Brazil for sponsoring Ms. Azevedo's PhD grant, and project PCTI/EQU 32470/99, the Ministry of Science and Technology of Portugal, for providing financial support for this research.

## Notation

$C$ = fluid-phase concentration, mol/void volume in bed
$C^{in}$ = bed inlet concentration, mol/m$^3$
$\overline{C}_p$ = mean pore concentration, mol/fluid volume in particle pores
$D_c$ = column diameter, m
$D_{pe}$ = effective pore diffusivity, m$^2$/s
$K$ = equilibrium constant, (mol. adsorbed/particle vol.)/(fluid vol. in particle pores/mol. in pore fluid phase)
$K'$ = equilibrium constant for a homogeneous adsorbent particle, (mol. adsorbed/particle vol.)/(void vol. in bed/mol. in bed fluid phase)
$k_h$ = mass-transport coefficient (LDF), s$^{-1}$
$k_f$ = film mass-transfer coefficient, m/s
$k_p$ = mass-transport coefficient in the pores, s$^{-1}$
$k_\mu$ = mass-transport coefficient in the microparticles, s$^{-1}$
$L_c$ = column length, m
$L_j$ = zone length, m
$m_2, m_3$ = ratio between liquid and solid net flow rates in TMB sections 2 and 3, respectively
$<\bar{q}>$ = mean solid-phase concentration averaged over the particle (bi-LDF approximation), mol adsorbed/particle volume
$\bar{q}$ = adsorbed concentration (homogeneous solid) averaged over the particle volume (LDF approximation), mol adsorbed/particle volume
$\bar{q}^*$ = concentration at the particle (homogeneous solid) surface in equilibrium with bulk fluid-phase concentration, mol adsorbed/particle volume
$Q$ = SMB fluid flow rate, m$^3$/s
$Q'$ = TMB fluid flow rate, m$^3$/s
$R_p$ = particle radius, m
$t^*$ = rotation period, s
$U_F$ = fluid interstitial velocity, m/s
$U_S$ = solid interstitial velocity, m/s
$V_c$ = column volume, m$^3$

### *Greek letters*

$\alpha_p$ = number of macropore mass-transfer units (bi-LDF approximation)
$\alpha_\mu$ = number of microparticle mass-transfer units (bi-LDF approximation)
$\alpha$ = number of mass-transfer units for a homogeneous adsorbent particle (LDF approximation)
$\epsilon$ = bed porosity, dimensionless
$\epsilon_p$ = particle porosity, dimensionless
$\nu$ = solid/fluid volume ratio
$\rho_p$ = particle density, kg/m$^3$

### *Superscripts and subscripts*

1, 2, 3, 4 = subscripts referring to TMB zones $c$ = column
$F,R,E,X$ = feed, raffinate, eluent, and extract SMB streams, respectively
$FR$ = fructose
$GL$ = glucose
$i$ = chemical species (fructose or glucose)
$j$ = TMB/SMB section
$k$ = SMB column
$p$ = particle

## Literature Cited

Azevedo, D. C. S., and A. E. Rodrigues, "Obtainment of High-Fructose Solutions from Cashew (Anacardium occidentale) Apple Juice by SMB Chromatography," *Sep. Sci. Technol.*, **35**, 2561 (2000).

Azevedo, D. C. S., and A. E. Rodrigues, "Design of a Simulated Moving Bed in the Presence of Mass Transfer Resistances," *AIChE J.*, **45**, 956 (1999a).

Azevedo, D. C. S., and A. E. Rodrigues, "Bi-Linear Driving Force Approximation in the Modeling of Simulated Moving Bed Using Bidisperse Adsorbents," *Ind. Eng. Chem. Res.*, **38**, 3519 (1999b).

Beste, Y. A., M. Lisso, G. Wozny, and W. Arlt, "Optimization of Simulated Moving Bed Plants with Low Efficient Stationary Phases: Separation of Fructose and Glucose," *J. Chromatog. A*, **868**, 169 (2000).

Broughton, D. B., and C. G. Gerhold, "Continuous Sorption Process Employing Fixed Bed of Sorbent and Moving Inlets and Outlets," U.S. Patent No. 2,985,589 (1961).

Broughton, D. B., H. J. Bieser, R. C. Berg, and E. D. Connel, "High Purity Fructose via Continuous Adsorptive Separation," *Suc. belg.*, **96**, 155 (1977).

Ching, C. B., C. Ho, and D. M. Ruthven, "An Improved Adsorption Process for the Production of High-Fructose Syrup," *AIChE J.*, **32**, 1876 (1986).

Ching, C. B., and D. M. Ruthven, "An Experimental Study of a Simulated Counter-Current Adsorption System: I. Isothermal Steady State Operation," *Chem. Eng. Sci.*, **40**, 877 (1985a).

Ching, C. B., and D. M. Ruthven, "An Experimental Study of a Simulated Counter-Current Adsorption System: II. Transient Response," *Chem. Eng. Sci.*, **40**, 887 (1985b).

Ching, C. B., and D. M. Ruthven, "Experimental Study of a Simulated Counter-Current Adsorption System: IV. Non-Isothermal operation," *Chem. Eng. Sci.*, **41**, 3063 (1986).

Gembicki, S. A., A. R. Oroskar, and J. A. Johnson, "Adsorption, Liquid Separation," *Encyclopedia of Separation Technology*, Vol. 1, D. M. Ruthven, ed., Wiley, New York, p. 172 (1997).

Hashimoto, K., S. Adachi, H. Noujima, and H. Maruyama, "Models for the Separation of Glucose/Fructose Mixture Using a Simulated Moving-Bed Adsorber," *J. Chem. Eng. Jpn.*, **16**, 400 (1983).

Hassan, M. M., A. K. M. Shamsur Rahman, and K. F. Loughlin, "Modeling of Simulated Moving Bed Adsorption System: A More Precise Approach," *Sep. Technol.*, **5**, 77 (1995).

Keller, G. E., II, "Adsorption: Building Upon a Solid Foundation," *Chem. Eng. Prog.*, **91**(10), 56 (1995).

Lameloise, M. L., and V. Viard, "Modeling and Simulation of a Glucose-Fructose Simulated Moving Bed Adsorber," *Trans. Inst. Chem. Eng.*, **71**, 27 (1993).

LeVan, M. D., "Adsorption Processes and Modeling: Present and Future," *Proc. Fundamentals of Adsorption (FOA6)*, F. Meunier, ed., Elsevier, Amsterdam, p. 19 (1998).

Ma, Z., and N.-H. L. Wang, "Standing Wave Analysis of SMB Chromatography: Linear Systems," *AIChE J.*, **43**, 2488 (1997).

Mallman, T., B. D. Burris, Z. Ma, and N.-H. L. Wang, "Standing Wave Design of Nonlinear SMB Systems for Fructose Purification," *AIChE J.*, **44**, 2628 (1998).

Mazzotti, M., G. Storti, and M. Morbidelli, "Robust Design of Countercurrent Adsorption Separation: 3. Nonstoichiometric Systems," *AIChE J.*, **42**, 2784 (1996).

Mazzotti, M., G. Storti, and M. Morbidelli, "Optimal Operation of Simulated Moving Bed Units for Nonlinear Chromatographic Separations," *J. Chromatog. A*, **769**, 3 (1997).

Migliorini, C., A. Gentilini, M. Mazzotti, and M. Morbidelli, "Design of Simulated Moving Bed Units under Nonideal Conditions," *Ind. Eng. Chem. Res.*, **38**, 2400 (1999).

Pais, L. S., J. M. Loureiro, and A. E. Rodrigues, "Modeling, Simulation and Operation of a Simulated Moving Bed for Continuous Chromatographic Separation of 1,1′-bi-2-Naphthol Enantiomers,"

*J. Chromatog. A*, **827**, 215 (1997).
Pais, L. S., J. M. Loureiro, and A. E. Rodrigues, "Modeling Strategies for Enantiomers Separation by SMB Chromatography," *AIChE J.*, **44**, 561 (1998).
Ruthven, D. M., *Principles of Adsorption and Adsorption Processes*, Wiley, New York (1984).
Storti, G., M. Mazzotti, M. Morbidelli, and S. Carrá, "Robust Design of Binary Countercurrent Adsorption Separation Processes," *AIChE J.*, **39**, 471 (1993).
Thoenes, D., Jr., and H. Kramers, "Mass Transfer from Spheres in Various Regular Packings to a Flowing Fluid," *Chem. Eng. Sci.*, **8**, 271 (1958).
Wooley, R., Z. Ma, and N.-H. L. Wang, "A Nine-Zone Simulating Moving Bed for the Recovery of Glucose and Xylose from Biomass Hydrolyzate," *Ind. Eng. Chem. Res.*, **37**, 3699 (1998).
Zhong, G., and G. Guiochon, "Analytical Solution for the Linear Ideal Model of Simulated Moving Bed Chromatography," *Chem. Eng. Sci.*, **51**, 4307 (1996).
Zhong, G., and G. Guiochon, "Steady-State Analysis of Simulated Moving-Bed Chromatography Using the Linear, Ideal Model," *Chem. Eng. Sci.*, **53**, 1121 (1998).
Zhong, G., M. Smith, and G. Guiochon, "Effect of the Flow Rates in Linear, Ideal, Simulated Moving Bed Chromatography," *AIChE J.*, **43**, 2960 (1997).

*Manuscript received Oct. 17, 2000, and revision received Mar. 20, 2001.*